ACS APPLIED MATERIALS & INTERFACES

Research Article

www.acsami.org

Nanostructuring of Iron Surfaces by Low-Energy Helium Ions

İrem Tanyeli,*[,†] Laurent Marot,[‡] Mauritius C. M. van de Sanden,[†] and Gregory De Temmerman[†]

[†]FOM-Institute, Dutch Institute for Fundamental Energy Research, Edisonbaan 14, 3439MN Nieuwegein, The Netherlands

[‡]Department of Physics, University of Basel, Klingelbergstrasse 82, Basel, Switzerland

ABSTRACT: The behavior of iron surfaces under helium plasma exposure is investigated as a function of surface temperature, plasma exposure time, and He ion flux. Different surface morphologies are observed for a large process parameter range and discussed in terms of temperature-related surface mechanisms. Surface modification is observed under low-He ion flux (in the range of 10^{20} m^{-2} s^{-1}) irradiation, whereas fiberlike iron nanostructures are formed by exposing the surface to a high flux (in the range of 10^{23} m^{-2} s^{-1}) of low-energy He ions at surface temperatures of 450−700 °C. The effects of surface temperature and plasma exposure time on nanostructures are studied. The results show that surface processing by high-flux low-energy He ion bombardment provides a size-controlled nanostructuring on iron surfaces.

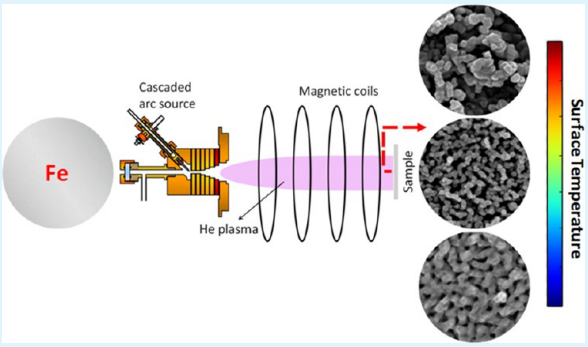

KEYWORDS: *surface modification, iron, He ion plasma*

INTRODUCTION

Nanoscale materials provide an enhanced activity with their high surface area to volume ratios in various applications, especially in light-driven processes. For instance, the efficiency of direct solar water splitting in photoelectrochemical cells is increased by nanostructuring the surface of metal oxides, which are used as photoelectrodes.[1,2] Because the metal oxides suffer from the mismatch between the light absorption depth and diffusion length of photogenerated charge carriers and also from the slow surface reaction kinetics, nanostructuring the surface is essential for overcoming these drawbacks. In addition, black metals, which have high absorption over a large portion of the solar spectrum, are good candidates in solar thermal and solar thermo-photovoltaic systems.[3−5] Hence, there has been strong interest in the development of efficient nanostructuring methods in recent decades. The majority of these methods are wet chemistry methods (spray pyrolysis techniques, solution-based colloidal methods, etc.[6,7]) and are competing in different aspects, such as time effectiveness, structure uniformities, and size limitations.

With regard to the disadvantages of wet chemistry methods, ion-assisted techniques have great potential in nanostructuring metal surfaces as being dry processes. Microstructural changes on metals induced by high-energy (in the range of kiloelectronvolts) ion bombardment have long been reported.[8,9] Irradiation by ions with energies above the threshold energy for displacement damage leads to radiation damage underneath the metal surface via the formation of interstitials and vacancies. However, recent studies showed that radiation-induced surface modifications can be obtained even with low-energy (<50 eV) helium ion irradiation.[10,11] It is claimed that once helium atoms diffuse beneath the metal surface, they tend to agglomerate and form bubbles.[12] These helium bubbles coalesce and thereby swell.[12] As a consequence of that, nanostructures are formed by extending the metal surface. Experimental studies showed that nanostructure formation is highly dependent on incident ion energy,[13] surface temperature,[12] and ion flux.[14] Although the process is not fully understood and has not yet been explained, a more detailed hypothesis about the formation of helium-induced nanostructures can be found in refs 12 and 15. Most of the experimental and theoretical studies have been conducted on tungsten.[16−18] The porosity of tungsten surfaces after helium plasma exposure reaches 90%, which implies a very high light absorption, almost 99% across the whole visible spectrum.[19] Similar helium-induced morphology changes were observed on different metal surfaces, such as molybdenum, titanium, and iron.[11,20] It was recently demonstrated that helium plasma processing of tungsten followed by a two-step oxidation procedure allowed the formation of porous tungsten oxide with good photocatalytic activity.[21] This demonstrates the potential of helium ion irradiation for surface nanostructuring.

There has been growing interest in the iron oxide photoanodes in photoelectrochemical water splitting.[1] Iron(III) oxide provides higher light absorption, namely a higher solar to hydrogen (STH) conversion efficiency, than the other competing metal oxides, such as WO_3 and TiO_2, because of its smaller bandgap.[1] In addition to that, its stability in aqueous environments and low cost make it a promising material for solar hydrogen production. However, the efficiency is limited by the poor charge carrier transport in iron oxide;[1] thus, the surface needs to be nanostructured. Our study provides

Received: December 6, 2013
Accepted: February 3, 2014
Published: February 3, 2014

   dx.doi.org/10.1021/am405624v | ACS Appl. Mater. Interfaces 2014, 6, 3462−3468

controllable nanostructure formation on iron surfaces with surface temperature and plasma exposure time. After oxidation, these structures can be used as photoanodes for solar water splitting. All the processes starting from nanostructuring a mirror finish polished surface under a high flux of low-energy He ion irradiation to oxidizing to the desired oxide phase for solar water splitting have been demonstrated in principle for tungsten.[21]

In this study, we study the bottom-up nanostructuring of iron surfaces by exposure to helium plasma. Helium-induced modifications of the iron surface have recently been studied by Kajita et al.[20] However, in this study, we present a detailed investigation of the surface modification of iron under a large parameter range and as a means of developing controlled nanostructure growth. Iron surfaces were irradiated using two different flux regimes within a broad temperature range for different plasma exposure times. In this work, the effect of these parameters on surface modification will be discussed.

EXPERIMENTAL SECTION

Polycrystalline iron samples (99.8% pure, Good Fellow) were exposed to helium plasma within a large range of ion fluxes (1×10^{20} to 6.5×10^{23} m^{-2} s^{-1}). High-flux irradiation was conducted in the Pilot-PSI linear plasma generator (Figure 1). The plasma is generated by a

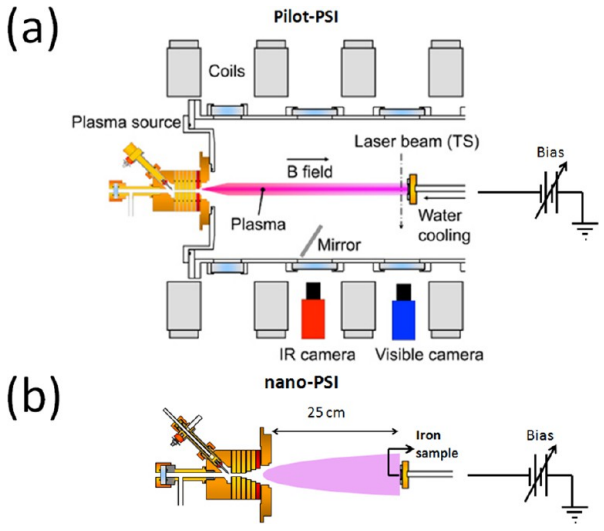

Figure 1. Schematic view of the Pilot-PSI (a) and nano-PSI (b) setups.

cascaded arc source that exhausts into a 50 cm diameter vacuum vessel. The plasma jet is confined by an axial magnetic field. A detailed description of the setup can be found elsewhere.[22]

The magnetic field was set to 0.2 T during the experiments. Typical radial profiles of the electron temperature (T_e) and density (n_e) of the plasma beam, as measured by Thomson scattering (TS) at 17 mm in front of the target, are shown in Figure 2. The plasma beam has a Gaussian shape, and the maximal ion flux during exposures was in the range of $3.7–6.5 \times 10^{23}$ m^{-2} s^{-1}. The samples are fixed onto a water-cooled target holder using a clamping ring made out of molybdenum (Mo), and the distance between the plasma source and the sample surface is 54 cm. A layer of Grafoil is inserted between the holder and the sample to provide a better thermal contact. Surface heating is induced by the incoming plasma flux, and the surface temperature is regulated by water cooling. The samples are negatively biased with respect to the plasma potential to control the ion energy, which is set to 25 eV during the exposures.

Polycrystalline iron samples, which are 19 mm in diameter and 1 mm thick, were cut from a rod. These samples were mechanically polished with 320–2400 grit SiC papers and finalized to a mirror finish

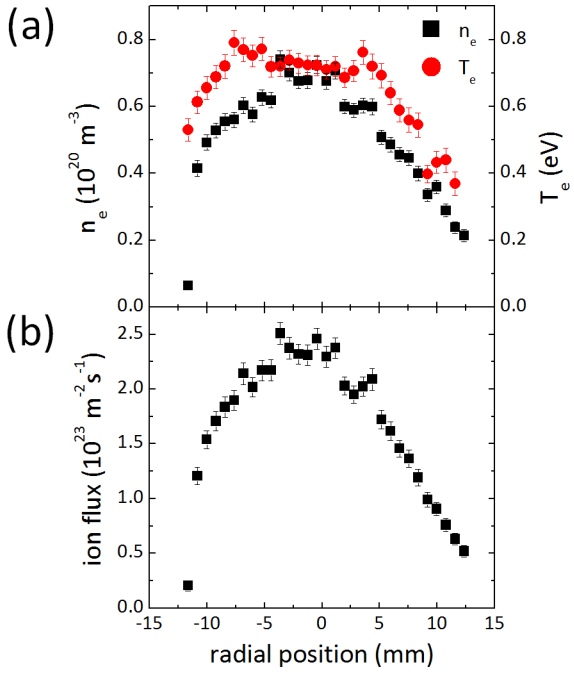

Figure 2. (a) Electron density (n_e) and temperature (T_e) and (b) ion flux density profiles of the helium plasma beam in the Pilot-PSI obtained via Thomson scattering.

by 3 to 1 μm diamond and 0.05 μm alumina suspensions. Polished samples were cleaned with acetone, ethanol, and deionized water in an ultrasonic bath, while the acetone step was repeated at the end to easily remove the remaining water droplets on the surfaces. The diameter of the plasma-exposed area of the samples is larger than the full width at half-maximum (fwhm) of the beam, which is around 15 mm. Hence, the surface temperature profile has a Gaussian shape. The peak temperature was measured by a multiwavelength pyrometer (FMPI SpectroPyrometer, FAR Associates), which measures in the wavelength range of 900–1600 nm. In addition, the two-dimensional surface temperature profile was measured with an infrared camera (FLIR A645 sc). The surface emissivity was determined by cross calibrating the measurements from both the pyrometer and the IR camera. The surface is modified by ions during the plasma exposure; hence, the emissivity value changes. The emissivity of iron was found to be 0.19 at the beginning of the exposure and changed to 0.22 at the end of the exposure for surface temperatures of around 450 °C, and when the surface temperature reached 700 °C, the emissivity increased to 0.26.

Low-ion flux exposures were performed in an expanding thermal plasma setup called a nano-PSI (Figure 1b).[23] As for the Pilot-PSI, a cascaded arc source is used to generate the plasma, which is freely expanding into a spherical vessel with a diameter of approximately 50 cm. The sample holder is positioned in the center of the spherical vessel; the diameter of the expanding plasma is larger than the diameter of the sample surface. This implies that there is no need to consider a spatial gradient for the ion flux or surface temperature. The sample can be actively heated or cooled with water so that the sample temperature is varied in a manner that is independent of the incident plasma flux. The sample temperature is measured by a K-type thermocouple, which is inserted through a hole at the side of the sample. Similarly to what is done in the Pilot-PSI, the ion energy is set to 25 eV by applying a negative bias potential to the samples. A double-Langmuir probe, which is 0.25 mm in diameter and 13.5 mm in length, is used to determine T_e and n_e. The measurements gave a T_e of ~0.3 eV and an n_e of $\sim 3.7 \times 10^{17}$ m^{-3}. The ion flux is calculated to be $\sim 1.3 \times 10^{20}$ m^{-2} s^{-1} at the beam center, and the beam fwhm was measured to be ~5 cm, i.e., much larger than the sample diameter.

After plasma exposures, the samples were analyzed by high-resolution scanning electron microscopy (SEM) to investigate the

dx.doi.org/10.1021/am405624v | ACS Appl. Mater. Interfaces 2014, 6, 3462–3468

surface morphology changes and by X-ray photoelectron spectroscopy (XPS) to study the surface composition.

RESULTS AND DISCUSSION

Panels a and b of Figure 3 show the surface modifications on iron samples after high-flux (3−4 × 10^{23} m^{-2} s^{-1}) He ion

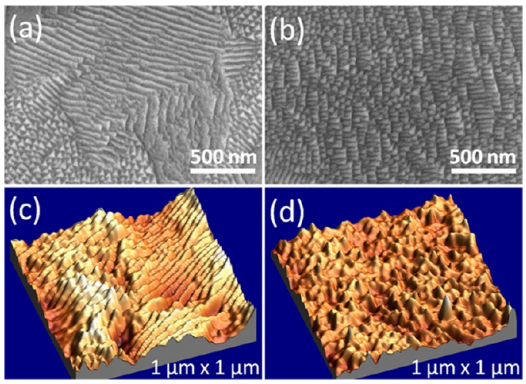

Figure 3. SEM images of iron surfaces exposed to He plasma (ion flux of 3−4 × 10^{23} m^{-2} s^{-1}) with surface temperatures of 130 °C for 5 min (a) and 200 °C for 20 min (b). AFM images of an iron surface exposed to He plasma with a surface temperature of 130 °C for 5 min taken 5−6 mm from beam center (c) and from the beam center (d).

irradiation, with surface temperatures of 130 °C for 5 min and 200 °C for 20 min, respectively. Ripples with a height of 3−10 nm, as measured by AFM (Figure 3c), are observed on these surfaces. The ions hit the surface with an energy of 25 eV, which is slightly above the sputtering threshold energy for iron by He ions (≈24.22 eV).[25] The ripple orientation appears to depend on the grain orientation. In that sense, the formation of such structures is consistent with Bradley Harper's model,[26] which is based on Sigmund's sputtering theory.[27] Moreover, the contribution from sputtering by impurities cannot be neglected. Some experimental studies reported that ripple formation is aided by destabilization of the surface by sputter codeposition of impurity materials.[28,29] From XPS analysis, we have detected some traces of molybdenum in the region where we observe ripples. The most likely candidate for the source of Mo contamination in our experimental setup is the clamping ring. Although the sputtering threshold energy for Mo by He ions (≈59 eV) is quite above the energy imposed by biasing in our case,[25] the enhancement of the localized electric field around the sharp regions of our clamping ring could cause sputtering. It should be noted that surface modifications by the formation of a wavy structure have been reported for the case of tungsten surfaces after irradiation by a high flux of low-energy He ions with energies below the sputtering threshold of tungsten.[24] Those structures were accompanied by the formation of pinholes on the surface, and it is not entirely clear that the same process is occurring in the case of iron, where pinholes cannot be observed. It is worth noting that, in this case, these structures are not observed at the location of the highest heat flux (Figure 3d) but are found 5−6 mm from the beam center, i.e., almost at the edge of the plasma beam. Vasiliu et al. observed a similar situation in iron samples irradiated by high-energy (in the kiloelectronvolt range) Ar ions.[30] They claimed that there is a defect and dislocation flow from the center of the beam to the edge where temperature and ion flux gradients exist.

Panels a and b of Figure 4 show SEM images of iron samples exposed to He plasma with a flux of 3.5 × 10^{23} m^{-2} s^{-1} at

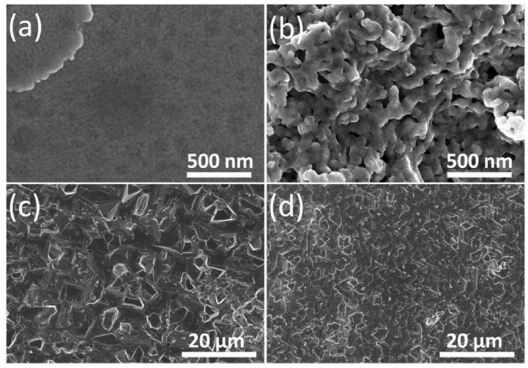

Figure 4. SEM images of iron surfaces after He plasma exposure at 270 (a), 450 (b), 780 (c), and 940 °C (d) with an ion flux of 3.5 × 10^{23} m^{-2} s^{-1}.

surface temperatures of 270 and 450 °C, respectively. The ripples, which we observe up to a surface temperature of 200 °C, disappear, and no periodic or continuous structures exist on the surface. At a surface temperature of 450 °C, some holes begin to appear on the surface as shown in Figure 4b. Organized helium-induced nanostructure formation starts above 450 °C, and fiberlike nanostructures are observed up to 700 °C. Iron surfaces after helium plasma exposure with an ion flux of 3.5−6.5 × 10^{23} m^{-2} s^{-1} in that temperature range are shown in Figure 5. As shown in the first SEM images of each row in Figure 5, a networklike structure is observed on the surface. With the increase in the surface temperature, nanosized structures appear on the surface. Once these structures form, their characteristic size increases with temperature. The individual structure size for a 5 min exposure with a surface temperature of 570 °C is around 100−200 nm in diameter, whereas for longer exposures, the nanostructures become finer with a diameter of around 50−100 nm. To gain quantitative insight into how the size of nanostructures is affected by the surface temperature and exposure time, SEM images in Figure 5 were analyzed using Gwyddion.[31]Because the structures are randomly shaped, instead of having a mean diameter, the mean grain area was plotted against the surface temperature for three different exposure times in Figure 6. The mean grain area covered by iron nanostructures increases with surface temperature for all three different plasma exposure times. It is also worth pointing out that the individual structure sizes and mean grain areas of iron nanostructures formed under plasma irradiation with surface temperatures of around 700 °C for both 20 and 60 min exposures are very close to each other; in fact, the structures seem not to evolve further after exposure for 20 min. With a further increase in temperature, we could mention that recrystallization might affect the mechanisms for surface modification as seen in panels c and d of Figure 4, i.e., for surfaces exposed to a surface temperature of >780 °C. For pure iron, the recrystallization temperature is around 450 °C, a temperature that can be higher for less pure iron grades.[32]

We already observed the upper limit of He ion fluence for nanostructure formation as shown in Figure 5. To investigate the lower boundary for He-induced surface modification, iron surfaces were exposed to a low flux of He ions, on the order of 10^{20} m^{-2} s^{-1}. The surface temperature was set to 300 °C, where nanostructuring is not observed for samples exposed in the

dx.doi.org/10.1021/am405624v | ACS Appl. Mater. Interfaces 2014, 6, 3462−3468

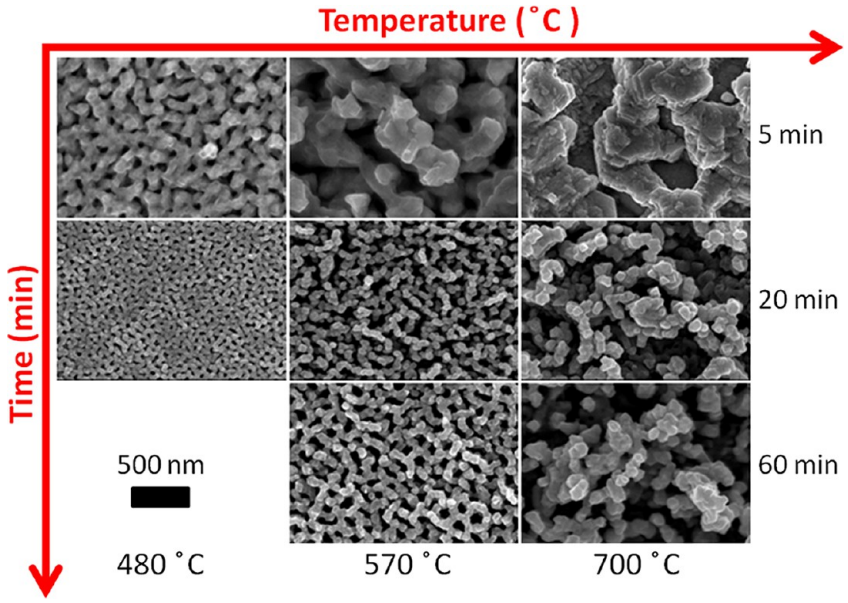

Figure 5. Evolution of He-induced nanostructure formation on an iron surface for three different exposure times with an ion flux of 3.5−6.5 × 10^{23} m^{-2} s^{-1}.

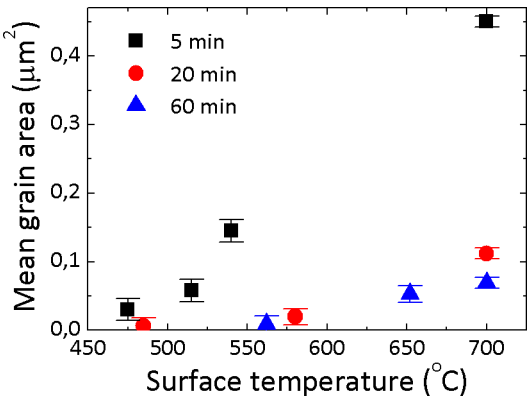

Figure 6. Mean grain area vs surface temperature.

high-flux regime (see Figure 4), and to 600 °C, where fine nanostructures form under high-ion flux irradiation (see Figure 5). The iron surfaces exposed with surface temperatures of 300 and 600 °C for 1 h in the nano-PSI are shown in Figure 7. The

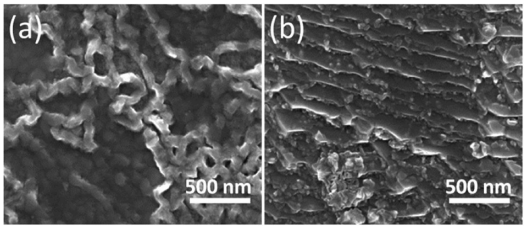

Figure 7. Surface modification of iron exposed to 4.7 × 10^{23} m^{-2} He fluence (1 h) with surface temperatures of 300 (a) and 600 °C (b).

surfaces at both temperatures are affected by plasma irradiation. Instead of fine nanostructures, we observe random nanostructures on both iron surfaces that were exposed at 300 and 600 °C. The nanostructure growth from the surface, for tungsten and molybdenum, is attributed to the formation of pressurized bubbles,[33,34] and a sufficient ion fluence is needed. In general, our exposures on iron samples from different flux regimes indicate that there is a threshold He ion fluence for He ion-induced nanostructure growth on iron. Similarly but more extensively, the effects of ion energy[12] and ion flux[14] on the growth kinetics of a nanostructured layer on a tungsten surface have been reported.

Figures 4 and 5 revealed that there is a strong correlation among the surface temperature, ion fluence, and surface modification. During nanostructure formation, different mechanisms are used, such as ion erosion, helium ion diffusion, surface diffusion, volume viscous flow, void formation, and recrystallization. One or several of these competing mechanisms become dominant depending upon the temperature range and ion fluence. The formation of ripples indicated that ion erosion may be a process in the low-temperature range, around 150−200 °C in our experiments (Figure 3). Moreover, with an increase in temperature, the mechanisms, which are driven by temperature, may become predominant. For instance, surface diffusion becomes more rapid. The temperature dependence of self-diffusion coefficients in bcc Fe was plotted starting from 227 °C in a study by Mendelev and Mishin.[35] They showed that it follows an Arrhenius-type behavior. With an increase in temperature, the surface kinetics may be taken over by surface smoothing, which is driven by the decrease in surface energy. Beyond 450 °C, a well-organized surface modification starts to be observed (Figure 5). When the surface temperature is further increased, nanostructures with a diameter of 100−200 nm tend to grow from the surface. These structures were analyzed by TEM to gain more insight into their inner structure (Figure 8). As seen in Figure 9, pores are detected in the near surface with sizes of <20 nm. Similarly, in the cross section view of the structures shown in Figure 9a, pores are visualized. Pinholes can be observed for different parts of the surface (Figure 9b) that are exposed to different ion fluxes because of the Gaussian plasma profile. For tungsten, it was shown that pinholes are formed during the earlier stages of nanostructure formation under He ion irradiation[36] and precede the formation of the rodlike structure.

dx.doi.org/10.1021/am405624v | ACS Appl. Mater. Interfaces 2014, 6, 3462−3468

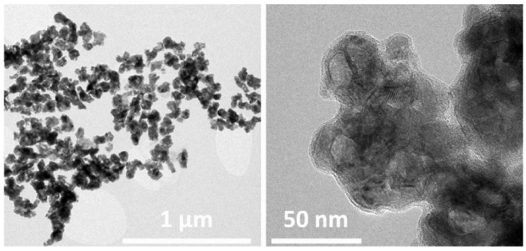

Figure 8. TEM images taken from nanostructures formed after plasma exposure at 700 °C for 20 min.

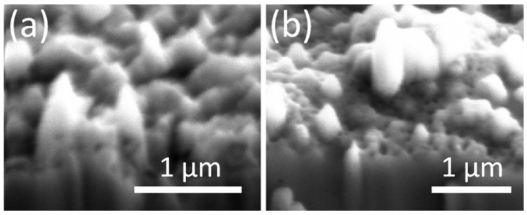

Figure 9. Pores are detected both inside the nanostructures (a) and in the outer part of the beam center (b).

The force by pressurized He bubbles leads to a viscous flow of metal from the surface.[15] Once these structures form, they grow with an increase in temperature. Stewart et al. simulated the formation and diffusion of He clusters and bubbles in iron for temperatures of up to 927 °C.[37] They showed that the diffusion rate of helium interstitials and clusters increases with temperature. As a consequence of that, helium bubbles coalesce rapidly, and this leads to larger features. We observe a similar trend in our experimental results. The presence of voids underneath the surface indicates that there is a similarity in nanostructure formation on iron, tungsten, and molybdenum surfaces; all three are bcc metals. However, the thickness of the nanostructured layer was found to be around 500 nm, which is much thinner than what is typically observed on tungsten or molybdenum with similar exposure times. The nanostructured layer thickness on tungsten surfaces, which were exposed at 1000, 1500, and 2000 °C for 500 and 1000 s, was around 1−2 μm.[11] This implies that there has to be another process that limits the nanostructured layer growth on iron. When we consider our experimental conditions, the most likely candidate that could decelerate the growth process on the iron surface seems to be physical sputtering. The effect of physical sputtering on the nanostructured layer growth on the tungsten surface was studied by Doerner et al. by bombarding the surface at different incident ion energies.[18] No net erosion yield was detected after the exposures at energies well below the threshold for physical sputtering of tungsten by helium; hence, the growth rate of the nanostructured layer revealed its inverse square root of time dependence as shown in one of their previous studies.[16] They achieved a stationary nanostructured layer thickness under stronger energetic ion irradiation due to the fact that the growth rate and sputtering rate compete and reach a balance. The ion energy in our study is slightly above the threshold energy for iron sputtering by helium ions. Hence, we can expect to observe sputtering on the iron surface, whereas the effect of sputtering is negligible in the case of tungsten. To verify that assumption, we measured the mass of our samples before and after plasma exposures. From those mass loss measurements, the sputtering yield (Y) can be calculated by

$$Y = \frac{\Delta m}{M_2 n_1} N_0 \quad (1)$$

where Δm is the mass change, M_2 is the iron's atomic mass, n_1 is the number of He ions reaching the surface, and N_0 is Avogadro's number. The plot of the measured sputtering yield versus ion fluence is seen in Figure 10. The sputtering yield

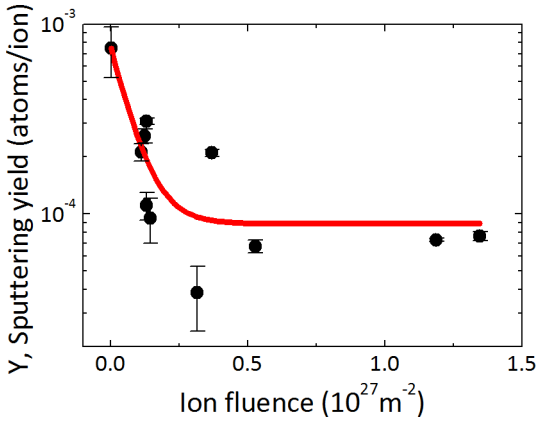

Figure 10. Sputtering yield vs ion fluence.

decreases with ion fluence and reaches a steady state regime for ion fluencies of >3 × 10^{26} m^{-2}. Nishijima et al. bombarded their nanostructured tungsten surfaces with Ar ions.[38] In that study, they detected a clear decrease in the sputtering yield of the porous surface compared to the yield measured for the smooth surface. Consistent with that, in our case the end of the rapid decrease in the sputtering yield corresponds to the region where we obtain nanostructured surfaces with a porous surface. In general, it can be noted that the dependency of the nanostructure growth kinetics on surface temperature and plasma exposure time for iron surfaces is consistent with the results from tungsten and molybdenum surfaces,[11] which might indicate that a similar mechanism is active.

To gain insight into the chemical composition of our samples, they were analyzed by XPS. The measurements were taken from polished iron surfaces before and after plasma exposure (Figure 11). Both unexposed and plasma-exposed iron surfaces show elemental iron (Fe $2p_{1/2}$ and Fe $2p_{3/2}$ at binding energies of 719.9 and 706.8 eV, respectively) and iron oxide (Fe $2p_{1/2}$ and Fe $2p_{3/2}$ at binding energies of 724.6 and 710.9 eV, respectively) at levels consistent with literature

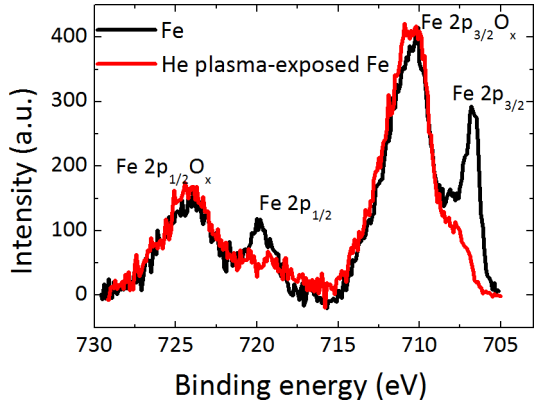

Figure 11. XPS of reference iron and plasma-exposed iron.

dx.doi.org/10.1021/am405624v | ACS Appl. Mater. Interfaces 2014, 6, 3462−3468

values.[39] Both samples show the expected ratio of Fe $2p_{3/2}$ to Fe $2p_{1/2}$ of 2:1. Figure 11 shows the iron oxide content to be higher in the plasma-exposed surface than in the unexposed one. Assuming that the single overlayer model can be used to quantify the iron oxide to iron elemental ratio, the exposed sample shows approximately twice the amount of iron oxide compared to the unexposed sample. The difference in the oxidation might be attributed to the increased surface area after plasma exposure, namely a larger reactive area with oxygen. A significant contribution due to different morphologies cannot be excluded. Considering the slight shifts in the peak positions for our measurements and the reference article, the oxide phase on our samples is possibly a nonstoichiometric structure between Fe_2O_3 and Fe_3O_4. For applications in solar water splitting, the Fe_2O_3 phase is desired and future work will concentrate on the development of stoichiometric oxides after nanostructuring by helium ions. A proof of principle of this approach has recently been reported by de Respinis et al.[21]

CONCLUSION

The effect of helium plasma treatment of iron surfaces has been studied. Control over nanostructure formation is achieved by surface temperature and plasma exposure time. Pressurized helium bubble-induced surface morphology changes are clearly observed under high-flux ($3-6.8 \times 10^{23}$ m^{-2} s^{-1}) irradiation. Controlled nanostructure formation is achieved between 450 and 700 °C. The nanostructures become larger with an increase in surface temperature and become finer with an increase in plasma exposure time until they reach the saturation limit in ion fluence. Fine nanostructures, which are around 50 nm in diameter and 500 nm in length, are grown on the iron surface after a high flux of low-energy He ions at 700 °C for 20 min. Despite some differences in the nanostructure growth kinetics of iron and tungsten, the dependency of the feature size on surface temperature shows consistency, indicating that the mechanisms of helium-induced modifications might be similar for those metals.

AUTHOR INFORMATION

Corresponding Author

*E-mail: i.tanyeli@differ.nl.

Notes

The authors declare no competing financial interest.

ACKNOWLEDGMENTS

We thank Erwin Zoethout for XPS measurements and Osman El-Atwani for cross section images. This work is part of the research program of the Stichting voor Fundamenteel Onderzoek der Materie (FOM), which is financially supported by the Nederlandse Organisatie voor Wetenschappelijk Onderzoek (NWO). It is supported by the European Communities under the contract of Association between EURATOM and FOM and was conducted within the framework of the European Fusion Programme.

REFERENCES

(1) Sivula, K.; Le Formal, F.; Grätzel, M. Solar Water Splitting: Progress Using Hematite (α-Fe_2O_3) Photoelectrodes. *ChemSusChem* **2011**, *4*, 432−449.

(2) Berger, S.; Tsuchiya, H.; Ghicov, A.; Schmuki, P. High photocurrent conversion efficiency in self-organized porous WO_3. *Appl. Phys. Lett.* **2006**, *88*, 203119-1−203119-3.

(3) Nagpal, P.; Han, S. E.; Stein, A.; Norris, D. J. Efficient Low-Temperature Thermophotovoltaic Emitters from Metallic Photonic Crystals. *Nano Lett.* **2008**, *8* (10), 3238−3243.

(4) Rephaeli, E.; Fan, S. Tungsten black absorber for solar light with wide angular operation range. *Appl. Phys. Lett.* **2008**, *92*, 211107-1−211107-3.

(5) Ungaro, C.; Gray, S. K.; Gupta, M. C. Black tungsten for solar power generation. *Appl. Phys. Lett.* **2013**, *103*, 071105-1−071105-3.

(6) Duret, A.; Grätzel, M. Visible Light-Induced Water Oxidation on Mesoscopic α-Fe_2O_3 Films Made by Ultrasonic Spray Pyrolysis. *J. Phys. Chem. B* **2005**, *109* (36), 17184−17191.

(7) Brillet, J.; Grätzel, M.; Sivula, K. Decoupling Feature Size and Functionality in Solution-Processed, Porous Hematite Electrodes for Solar Water Splitting. *Nano Lett.* **2010**, *10* (10), 4155−4160.

(8) Sakamoto, R.; Muroga, T.; Yoshida, N. Microstructural evolution induced by low energy hydrogen ion irradiation in tungsten. *J. Nucl. Mater.* **1995**, *220−222*, 819−822.

(9) Nakamura, Y.; Kitajima, S.; Shinohara, K. Influence of 100 keV helium irradiation on tensile properties of pure iron and JFMS steel at low temperatures. *J. Nucl. Mater.* **1989**, *169*, 185−197.

(10) Tokunaga, K.; Baldwin, M. J.; Doerner, R. P.; Noda, N.; Kubota, Y.; Yoshida, N.; Sogabe, T.; Kato, T.; Schedler, B. Blister formation and deuterium retention on tungsten exposed to low energy and high flux deuterium plasma. *J. Nucl. Mater.* **2005**, *337−339*, 887−891.

(11) De Temmerman, G.; Bystrov, K.; Zielinski, J. J.; Balden, M.; Matern, G.; Arnas, C.; Marot, L. Nanostructuring of molybdenum and tungsten surfaces by low-energy helium ions. *J. Vac. Sci. Technol., A* **2012**, *30*, 041306-1−041306-6.

(12) Kajita, S.; Sakaguchi, W.; Ohno, N.; Yoshida, N.; Saeki, T. Formation process of tungsten nanostructure by the exposure to helium plasma under fusion relevant plasma conditions. *Nucl. Fusion* **2009**, *49*, 095005-1−095005-6.

(13) Nishijima, D.; Ye, M. Y.; Ohno, N.; Takamura, S. Incident ion energy dependence of bubble formation on tungsten surface with low energy and high flux helium plasma irradiation. *J. Nucl. Mater.* **2003**, *313−316*, 97−101.

(14) Baldwin, M. J.; Doerner, R. P.; Nishijima, D.; Tokunaga, K.; Ueda, Y. The effects of high fluence mixed-species (deuterium, helium, beryllium) plasma interactions with tungsten. *J. Nucl. Mater.* **2009**, *390−391*, 886−890.

(15) Krasheninnikov, S. I. Viscoelastic model of tungsten 'fuzz' growth. *Phys. Scr.* **2011**, *T145*, 014040-1−014040-4.

(16) Baldwin, M. J.; Doerner, R. P. Helium induced nanoscopic morphology on tungsten under fusion relevant plasma conditions. *Nucl. Fusion* **2008**, *48*, 035001-1−035001-5.

(17) Nishijima, D.; Iwakiri, H.; Amano, K.; Ye, M. Y.; Ohno, N.; Tokunaga, K.; Yoshida, N.; Takamura, S. Suppression of blister formation and deuterium retention on tungsten surface due to mechanical polishing and helium pre-exposure. *Nucl. Fusion* **2005**, *45*, 669−674.

(18) Doerner, R. P.; Baldwin, M. J.; Stangeby, P. C. An equilibrium model for tungsten fuzz in an eroding plasma environment. *Nucl. Fusion* **2011**, *51*, 043001-1−043001-6.

(19) Kajita, S.; Saeki, T.; Yoshida, N.; Ohno, N.; Iwamae, A. Nanostructured Black Metal: Novel Fabrication Method by Use of Self-Growing Helium Bubbles. *Appl. Phys. Express* **2010**, *3*, 085204-1−085204-3.

(20) Kajita, S.; Yoshida, T.; Kitaoka, D.; Etoh, R.; Yajima, M.; Ohno, N.; Yoshida, H.; Yoshida, N.; Terao, Y. Helium plasma implantation on metals: Nanostructure formation and visible-light photocatalytic response. *J. Appl. Phys.* **2013**, *113*, 134301-1−134301-7.

(21) de Respinis, M.; De Temmerman, G.; Tanyeli, I.; van de Sanden, M. C. M.; Doerner, R. P.; Baldwin, M. J.; van de Krol, R. Efficient plasma route to nanostructure materials: Case study on the use of m-WO_3 for solar water splitting. *ACS Appl. Mater. Interfaces* **2013**, *5*, 7621−7625.

(22) De Temmerman, G.; Zielinski, J. J.; van Diepen, S.; Marot, L.; Price, M. ELM simulation experiments on Pilot-PSI using simulta-

neous high flux plasma and transient heat/particle source. *Nucl. Fusion* **2011**, *51*, 073008-1−073008-8.
(23) Bystrov, K.; Morgan, T. W.; Tanyeli, I.; De Temmerman, G.; van de Sanden, M. C. M. Chemical sputtering of graphite by low temperature nitrogen plasmas at various substrate temperatures and ion flux densities. *J. Appl. Phys.* **2013**, *114*, 133301-1−133301-11.
(24) Ohno, N.; Hirahata, Y.; Yamagiwa, M.; Kajita, S.; Takagi, M.; Yoshida, N.; Yoshihara, R.; Tokunaga, T.; Tokitani, M. Influence of crystal orientation on damages of tungsten exposed to helium plasma. *J. Nucl. Mater.* **2013**, *438*, S879−S882.
(25) Eckstein, W. In *Sputtering by Particle Bombardment*; Behrisch, R., Eckstein, W., Eds.; Topics in Applied Physics; Springer-Verlag: Berlin, 2007; Vol. *110*, Chapter Sputtering Yields, pp 33−187.
(26) Bradley, R. M.; Harper, J. M. E. Theory of ripple topography induced by ion bombardment. *J. Vac. Sci. Technol., A* **1988**, *6*, 2390−2395.
(27) Sigmund, P. Theory of Sputtering. I. Sputtering Yield of Amorphous and Polycrystalline Targets. *Phys. Rev.* **1969**, *184*, 383−416.
(28) Macko, S.; Frost, F.; Ziberi, B.; Förster, D. F.; Michely, T. Is keV ion-induced pattern formation on Si(001) caused by metal impurities? *Nanotechnology* **2010**, *21*, 085301-1−085301-9.
(29) Özaydin, G.; Özcan, A. S.; Wang, Y.; Ludwig, K. F.; Zhou, H.; Headrick, R. L.; Siddons, D. P. Real-time X-ray studies of Mo-seeded Si nanodot formation during ion bombardment. *Appl. Phys. Lett.* **2005**, *87*, 163104-1−163104-3.
(30) Vasiliu, F.; Teodorescu, I. A.; Glodeanu, F. SEM investigations of iron surface ion erosion as a function of specimen temperature and incidence angle. *J. Mater. Sci.* **1975**, *10*, 399−405.
(31) Klapetek, P.; Nečas, D. *Gwyddion*; Czech Metrology Institute: Brno, Czech Republic, 2007.
(32) Bugayev, K.; Konovalov, Y.; Bychkov, Y.; Kovalenko, V.; Tretyakov, E. *Iron and Steel Production*; Books for Business: New York, 2001.
(33) Evans, J. H. An interbubble fracture mechanism of blister formation on helium-irradiated metals. *J. Nucl. Mater.* **1977**, *68*, 129−140.
(34) Kajita, S.; Nishijima, D.; Ohno, N.; Takamura, S. Reduction of laser power threshold for melting tungsten due to subsurface helium holes. *J. Appl. Phys.* **2006**, *100*, 103304-1−103304-10.
(35) Mendelev, M. I.; Mishin, Y. Molecular dynamics study of self-diffusion in bcc Fe. *Phys. Rev. B* **2009**, *80*, 144111-1−144111-9.
(36) Kajita, S.; Sakaguchi, W.; Ohno, N.; Yoshida, N.; Saeki, T. Formation process of tungsten nanostructure by the exposure to helium plasma under fusion relevant plasma conditions. *Nucl. Fusion* **2009**, *49*, 095005-1−095005-6.
(37) Stewart, D.; Osetskiy, Y.; Stoller, R. Atomistic studies of formation and diffusion of helium clusters and bubbles in BCC iron. *J. Nucl. Mater.* **2011**, *417*, 1110−1114.
(38) Nishijima, D.; Baldwin, M. J.; Doerner, R. P.; Yu, J. H. Sputtering properties of tungsten 'fuzzy' surfaces. *J. Nucl. Mater.* **2011**, *415*, S96−S99.
(39) Kim, K. J.; Moon, D. W.; Lee, S. K.; Jung, K. H. Formation of a highly oriented FeO thin film by phase transition of Fe_3O_4 and Fe nanocrystallines. *Thin Solid Films* **2000**, *360*, 118−121.